Terrestrial VLF transmitter injection into the magnetosphere

M. B. Cohen[1] and U. S. Inan[1,2]

Received 1 June 2012; revised 15 June 2012; accepted 18 June 2012; published 9 August 2012.

[1] Very Low Frequency (VLF, 3–30 kHz) radio waves emitted from ground sources (transmitters and lightning) strongly impact the radiation belts, driving electron precipitation via whistler-electron gyroresonance, and contributing to the formation of the slot region. However, calculations of the global impacts of VLF waves are based on models of trans-ionospheric propagation to calculate the VLF energy reaching the magnetosphere. Limited comparisons of these models to individual satellite passes have found that the models may significantly (by >20 dB) overestimate amplitudes of ground based VLF transmitters in the magnetosphere. To form a much more complete empirical picture of VLF transmitter energy reaching the magnetosphere, we present observations of the radiation pattern from a number of ground-based VLF transmitters by averaging six years of data from the DEMETER satellite. We divide the slice at ∼700 km altitude above a transmitter into pixels and calculate the average field for all satellite passes through each pixel. There are enough data to see 25 km features in the radiation pattern, including the modal interference of the subionospheric signal mapped upwards. Using these data, we deduce the first empirical measure of the radiated power into the magnetosphere from these transmitters, for both daytime and nighttime, and at both the overhead and geomagnetically conjugate region. We find no detectable variation of signal intensity with geomagnetic conditions at low and mid latitudes ($L < 2.6$). We also present evidence of ionospheric heating by one VLF transmitter which modifies the trans-ionospheric absorption of signals from other transmitters passing through the heated region.

Citation: Cohen, M. B., and U. S. Inan (2012), Terrestrial VLF transmitter injection into the magnetosphere, *J. Geophys. Res.*, *117*, A08310, doi:10.1029/2012JA017992.

1. Introduction

[2] Ground based Very Low Frequency (VLF, 10–30 kHz) transmitters have been utilized for long distance communications since their initial development prior to World War I [*Watt*, 1967, p. 120]. Because VLF waves reflect efficiently off both the ground and the lower ionosphere (70–90 km altitude), and penetrate 10s of meters into seawater ($\sigma = 10^{-4}$ S/m) via the skin effect, they have developed into useful communications tools for surface ships and submerged submarines. VLF transmitters were also utilized for geo-location prior to the advent of the Global Positioning System [*Swanson*, 1983]. Today, there are ∼20 powerful VLF transmitters in operation worldwide, often transmitting with minimum shift keying modulation at a data rate of 200 baud, and radiating 10 s of kW to as much as 1 MW.

[3] The dominant source of VLF waves on Earth is the global distribution of lightning flashes [*Chrissan and Fraser-Smith*, 1996], each of which radiates strongly at these frequencies [*Uman*, 1987, p. 118]. Although guided to global distances with attenuation rates of a few decibels per megameter [*Davies*, 1990, p. 389], a small fraction of the radiated VLF energy is absorbed by the ionosphere, and propagates in the magnetospheric environment in the right hand circularly polarized whistler mode [*Storey*, 1953; *Helliwell*, 1965]. 'Whistlers' launched from lightning can be subsequently observed in the conjugate region if guided along field-aligned irregularities known as ducts, but may also propagate in a non-ducted mode which refract but do not precisely follow magnetic field lines. Whistler mode VLF emissions from lightning are known to interact with energetic electrons (>100 keV) in the radiation belts via gyroresonance, producing both free-running triggered emissions [*Helliwell*, 1965], and inducing electron precipitation onto the ionosphere [*Helliwell et al.*, 1973] via pitch angle scattering [*Peter and Inan*, 2007]. Lightning has been shown to play a role in energetic electron losses from the radiation belts [*Gemelos et al.*, 2009] and may contribute to the formation of the slot region between the two radiation belts [*Vampola*, 1977].

[4] Anthropogenic ELF/VLF transmissions made on the ground have also been shown to excite wave-particle interactions, including triggered emissions, both for VLF [*Helliwell*, 1965, p. 279] and ELF frequencies [*Helliwell and Katsufrakis*, 1974; *Gołkowski et al.*, 2008]. It has also

[1]Department of Electrical Engineering, Stanford University, Stanford, California, USA.
[2]Department of Electrical Engineering, Koc University, Istanbul, Turkey.

Corresponding author: M. B. Cohen, 350 Serra Mall, Room 356, Stanford, CA 94305, USA. (mcohen@stanford.edu)

0148-0227/12/2012JA017992

been suggested that VLF transmitters may trigger significant electron precipitation [*Inan et al.*, 1984; *Kulkarni et al.*, 2008] although a recent experiment to detect and quantify this precipitation [*Inan et al.*, 2007] may have been tainted by the effects of VLF scattering from the heated region above the transmitter [*Graf et al.*, 2011], whose effects may be broader than those originally earlier by *Inan* [1990] and *Rodriguez and Inan* [1994], and those from HF heaters [*Barr et al.*, 1985]. *Clilverd et al.* [2008] analyze the role of ducted and non-ducted propagation entering the magnetosphere from VLF transmitters, and find that non-ducted propagation is significant at $L < 1.5$.

[5] The role of continuously operating VLF transmitters in radiation belt losses remains a subject of uncertainty. *Abel and Thorne* [1998] estimated the contributions of lightning-generated whistlers, plasmaspheric hiss, and VLF transmitters, finding that VLF transmitters played a significant role in determining radiation belt lifetimes below L ~ 2.5, based on comparison with data from the 'Starfish' experiment. Those calculations, however, were based on relatively crude early theoretical models of the trans-ionospheric propagation, such as that in *Helliwell* [1965, p. 61], and also the relative occurrence rates of whistlers. Hiss and VLF transmitters were not based on comprehensive observational data.

[6] In an effort to validate these early models, *Starks et al.* [2008] found that certain model predictions consistently overestimate VLF transmitter amplitudes in space by at least 20 dB compared to the measured values on a small number of passes from multiple satellites. Nevertheless, that study also used only a limited number of individual passes, from several different satellites. It has been suggested that this VLF transmitter signal deficit may be due to scattering off irregularities in the ionosphere induced by the heating itself [*Bell et al.*, 2008], but the quantitative experimental evidence of this phenomenon remains limited. Modeling of the scattering process suggests that a small fraction of the 20 dB wave loss (3–6 dB) can be attributed to scattering from field-aligned irregularities [*Foust et al.*, 2010] although other studies suggest that the loss involved may be higher [*Shao et al.*, 2012].

[7] In another effort to compare predictions to observations, *Tao et al.* [2010] found that the Helliwell absorption curves overestimated the VLF wave absorption, and furthermore that rocket measurements of the *D*-region in combination with a full wave model suggest 60–100 dB less attenuation than predicted by the Helliwell curves, deepening the model-data discrepancy.

[8] With the theoretical models of trans-ionospheric propagation thus remaining unverified, we present here empirical observations of VLF transmitter injection into space, using direct measurements in the topside of the ionosphere. We utilize electric and magnetic field recordings from the DEMETER satellite [*Berthelier et al.*, 2006; *Parrot et al.*, 2006] which operated from August 2004 until December 2010, at altitudes between 660 and 700 km, in a sun-synchronous, nearly polar orbit, passing over a given region twice per day, at ~1000 and ~2200 local time. The recordings on DEMETER include a burst mode, which samples one component each of the horizontal electric and magnetic field at 40 kHz over locations of particular interest (such as seismically active zones), and a survey mode, which saves spectral data regularly over the entire globe, with spectral resolution of ~20 Hz, and time resolution of ~2 s.

[9] In this paper, we exclusively utilize survey mode data. *Parrot et al.* [2009, Figure 1] was the first to use this data set for VLF transmitter observations, creating a single global map of VLF wave amplitudes between 18 and 25 kHz, in which the transmitter zones can be clearly seen.

2. Observations

[10] Table 1 shows the VLF transmitters that we measure here. They span a range of *L*-shells, frequencies, and include both continuous and pulsed transmitters. The three pulsed transmitters form the Russian-operated 'Alpha' navigation system, an equivalent to the now decommissioned 'Omega' system [*Swanson*, 1983]. The transmission format is described later. The other transmitters operate with minimum shift keying (MSK) format, in which the transmitter alternates between two frequencies spaced out at one half of the baud rate, in this case ±50 Hz and 200 baud, respectively. The MSK bandwidth necessarily covers the entire spectrum over a ~200 Hz range. NWC is currently the only significant VLF transmitter south of the equator, but may also have the most impact on the radiation belts due in large part to its location [*Kulkarni et al.*, 2008; *Li et al.*, 2012]. In many of the subsequent figures, we thus focus on NWC as a representative example due to the particularly intense signal (1 MW radiated power) and resulting high SNR.

[11] Despite the reduced time resolution (2 sec) in survey mode, the speed of DEMETER (~7 km/sec) enables resolution of spatial features on the order tens of km, facilitated by more than six years of recordings during which DEMETER passed over a given location a large number of times. Figure 1 shows the averaged radiation pattern above the NWC transmitter, over a 6000 km square region, for both nighttime passes (top panels) and daytime passes (bottom left panel). The location directly above NWC is at the origin and indicated with a white dot on this (and subsequent) figure. The space above NWC is divided into 25 km square pixels, which is sufficient to resolve even finer scale features of the radiation pattern. In this figure, all the energy within ±200 Hz of the center frequency (19.8 kHz) is summed. Over the more than 6 years of DEMETER recordings, NWC transmitted nearly continuously, stopping only from early June 2007 until late January 2008 for maintenance, which has been excluded from the average pattern shown here.

[12] The bottom right panel shows the number of measurements in each 25 km grid point. We note that the satellite moves ~14 km in each survey mode period, so that in a given satellite pass, we may have two measurements in a single pixel, both of which are counted here. The scattering of the pass locations over the six year period is not perfectly uniform, but given the general smoothness of radiation pattern in the top plots, it seems that even the pixels with a comparatively small number of measurements have gotten enough for a reliable measurement of the radiated pattern from NWC. As will be discussed later, this fact is in part due to the consistency of the radiated signal as a function of time and geomagnetic conditions.

[13] The origin location in Figure 1 is directly above the location of NWC on the ground, but the anisotropic propagation through the ionospheric plasma bends the energy

Table 1. VLF Transmitters Observed in this Paper[a]

Call	Latitude	Longitude	f (kHz)	Mode	L-shell	Dip Angle	Declination
KRA	45.40	38.10	11.905*	pulsed	1.79	63.2	6.1
NOV	55.76	84.40	12.649*	pulsed	2.54	74.3	8.1
KOM	50.32	136.59	14.881*	pulsed	1.88	65.4	−11.6
HWU	46.70	1.23	18.300	MSK	1.87	62.2	−1.0
GBZ	52.91	−3.28	19.800	MSK	2.48	67.4	−3.8
NWC	−21.82	114.17	19.800	MSK	1.32	−55.3	0.5
ICV	40.92	9.73	20.270	MSK	1.51	56.6	1.1
HWV	48.54	2.58	20.900	MSK	2.00	63.9	−1.1
NPM	21.42	−158.15	21.400	MSK	1.14	38.0	9.9
JJI	32.04	130.81	22.200	MSK	2.46	67.9	0.5
DHO	53.08	7.61	23.400	MSK	2.46	67.9	0.5
NAA	44.65	−67.29	24.000	MSK	2.87	71.0	−12.2

[a]The three Russian Alpha transmitters (*) alternate between the three frequencies (the pattern is described later). The Geomagnetic L-shell, dip angle, and declination are at the location 80 km above the transmitter for the year 2009.

somewhat (though not perfectly) along the magnetic field lines, beginning at the altitude where the magnetic field dominates the propagation over collisions (∼80 km). The location of the magnetic field line traced from 80 km above the transmitter to the satellite altitude of 680 km is indicated with a black dot on the plot (and all subsequent plots), which in this case is reaches the 680 km altitude ∼430 km north of the point directly above NWC. The observed signal from NWC shows an intense region of radiation, very close to this field line location. There is no qualitative difference between the magnetic field and electric field, although the magnetic field recordings are less sensitive due to the intrinsic difficulties of measuring magnetic field in the magnetosphere.

[14] In addition to the main beam of radiation, there are a series of concentric rings of radiation, which arise from the interference between different Earth-ionosphere waveguide modes, whose pattern in the Earth-ionosphere waveguide maps upward into the magnetosphere. This feature has been observed in association with powerful thunderstorms [*Parrot et al.*, 2008]. Such features may be analogous to the three regimes of radiation observed from the HAARP heater as discussed by *Piddyachiy et al.* [2008]. Finally, there is a swath of radiation extending to the north (equatorward) of NWC, which arise in part from the magnetic field lines bending toward horizontal.

[15] Figure 2 shows the temporal and spatial properties of the NWC nighttime signal. The bottom right panel shows the innermost part of the radiation region above NWC, with a white circle marking a 150 km radius around the most intense area. During the life of DEMETER, excluding the NWC maintenance period, there were 193 passes in which at least one survey mode measurement was made within the 150 km circle shown. The average electric field amplitude in each of these passes is calculated and shown in Figure 2 (top left), as a function of year. There is a 10–15 dB variability in the signal strength. Although this period featured a decline in solar activity toward an extended minimum, there is no long term trend in the signal strengths as the solar activity changes. Figure 2 (top right) shows a distribution of the amplitudes of the 193 close DEMETER passes, showing ∼10 dB of variability. Figure 2 (bottom left) shows the

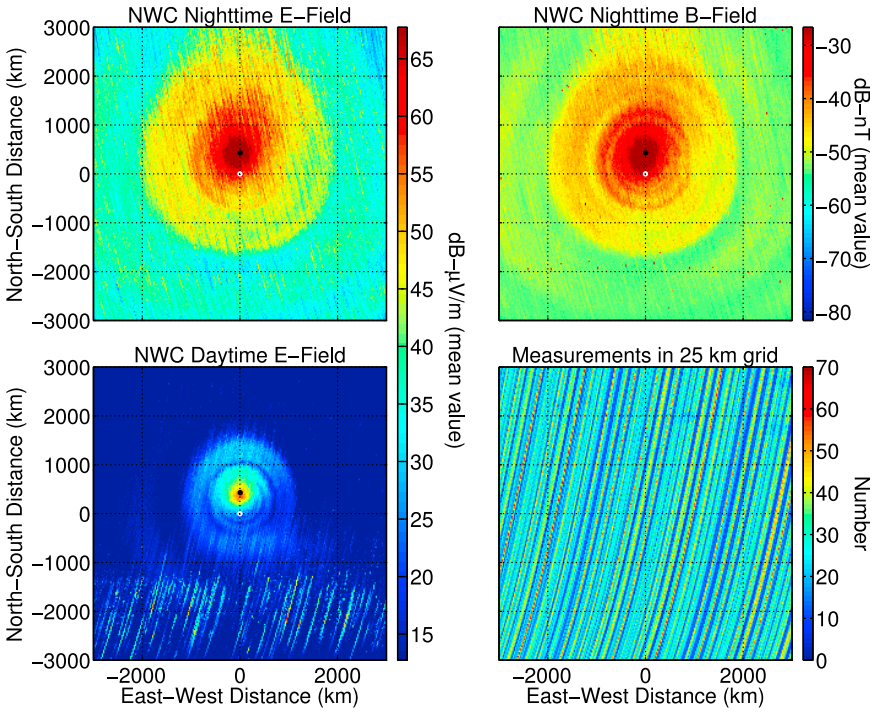

Figure 1. The radiation pattern from the NWC transmitter, as detected by DEMETER. (left) Electric field for (top) the nighttime passes and (bottom) daytime passes. (top right) Magnetic field data from the nighttime pass. (bottom right) The number of measurements in each 25 km grid cell. The black dots show the crossing point of the magnetic field line that begins at 80 km above the transmitter. The white dot at the origin is the location directly above the transmitter.

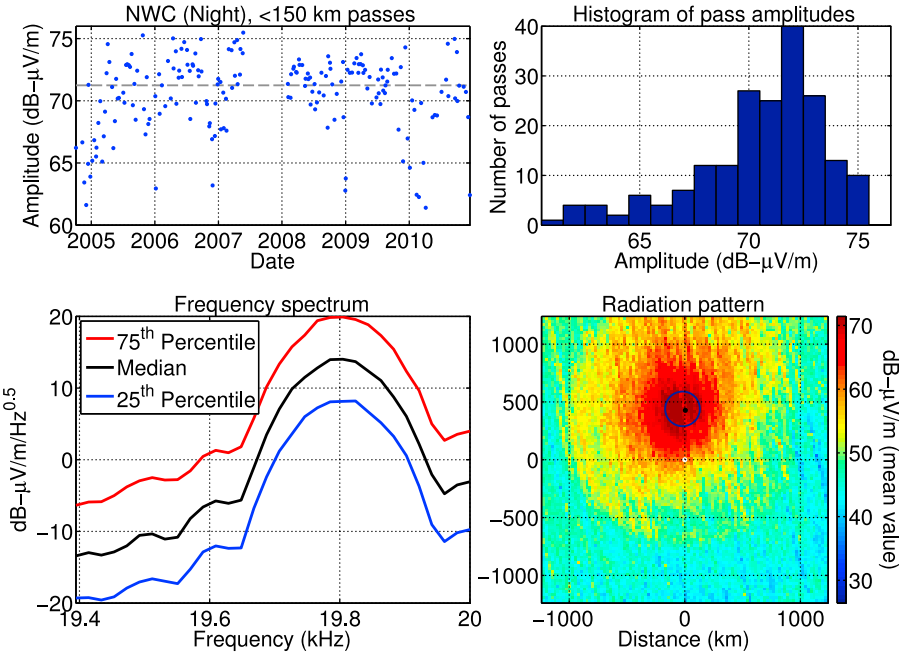

Figure 2. The NWC nighttime signal as a function of time and frequency. (bottom left) A 150 km circle around the center of the NWC radiation pattern, and this figure deals with the amplitudes and spectrum of signals within this circle. (top left) The average amplitude of each DEMETER pass through this region, over the entire 6-year mission, excluding a period in 2007 when the transmitter was off for maintenance. (top right) A histogram of the average amplitudes. (bottom left) The spectrum of the signal, including the median, 25th and 75th percentiles.

spectrum of the signal (∼20 Hz resolution), including the median and two quartile dividers. The spectrum has a 3 dB bandwidth of ∼150 Hz, with some energy detectable up to ±300 Hz total, which is mostly a direct product of the transmitted MSK energy. The variability in the received signal is ∼10 dB, which may be due to the varying ionospheric conditions from night to night.

[16] DEMETER also made measurements in the conjugate region to NWC, as shown in Figure 3, in which the space is again divided into 25 km pixels. The top row of panels show the nighttime measurements, the bottom row the daytime. In these plots, the origin is the location at the opposite end of the geomagnetic field line from NWC (L = 1.4) on the ground. The top row shows the nighttime measurements, the bottom row shows the daytime measurements. The two columns show the electric field (left) and magnetic field (right). To varying degrees the plots all show distinct regions of energy in the conjugate region, indicated with dashed ellipses in the figure. The smaller region, located ∼500 km south of the origin, is very close to the geomagnetic conjugate point of the most intense radiation spot seen in Figure 1. A second much larger region is located 500–1000 km poleward of the small region.

[17] The location of the larger region is less poleward in the nighttime magnetic field data compared to the electric field, but the two distinct regions can be seen in both day and night, and in both electric and magnetic field displays. A complete quantitative explanation of the two regions in the conjugate point is beyond the scope of this paper. Some factors to consider in interpretation of the conjugate signal may include the following: (1) Scattering off of irregularities as the signal emerges from the ionosphere, which changes the wave normal angles. The irregularities may be natural or generated by the transmitter. (2) Scattering off irregularities along the magnetospheric path. (3) The presence of ducts, either natural, or generated by the heater itself.

[18] One additional feature evident is a thin line of radiation, poleward shifted from the main transmitter signal, which closely follows the line of geomagnetic latitude for $L \sim$ =2.1.

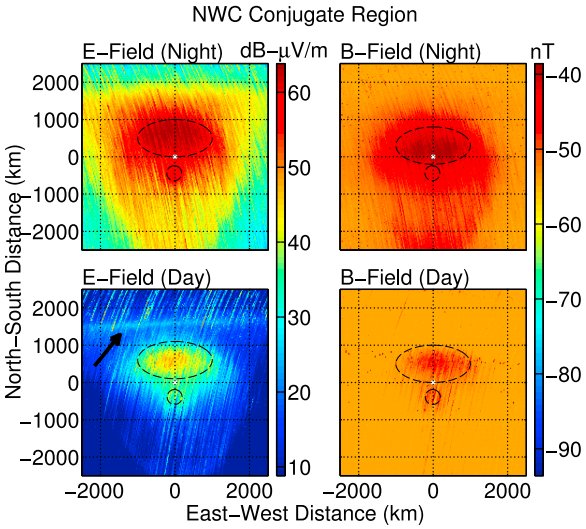

Figure 3. The averaged radiation pattern in the conjugate region. (top) The nighttime signals, (bottom) daytime signals, (left) electric field, and (right) magnetic field.

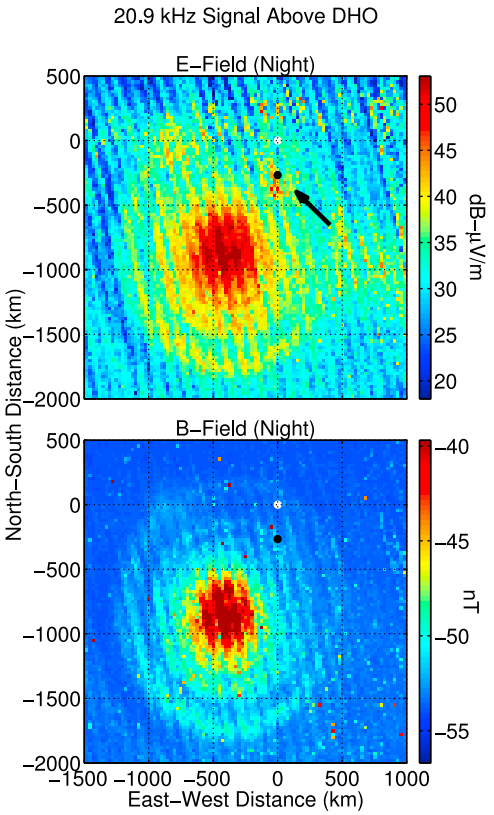

Figure 4. The radiation of 20.9 kHz ± 100 Hz (detected via aliasing at 19.1 kHz), in the region centered at the DHO transmitter (which broadcasts at 23.4 kHz). The white dot is the location of the DHO transmitter, and the black dot is the field line from 80 km altitude traced to 680 km.

It is indicated with an arrow in Figure 3 (bottom left). This latitudinal line is most evident and clear in the daytime E-field measurement, but is also more diffusely present in the nighttime E-field measurement, at roughly the same location. This feature may be due to a 'cusp' point, or an *L*-shell upper limit beyond which the magnetospherically reflected signal cannot cross. Resolution of this possibility is left to future workers.

[19] We also observe evidence of additional leakage of VLF energy through the ionosphere induced by the heated ionosphere above a second transmitter. Figure 4 shows the 20.9 kHz signal (detected via aliasing at 19.1 kHz) in the region above the DHO transmitter in Germany, for both electric field (top) and magnetic (bottom). The bandwidth used to generate these panels is ±100 Hz. The white dot is the location of the DHO transmitter, and the black dot is the field line of DHO from 80 km altitude traced to 680 km.

[20] We note that DHO transmits at 23.4 kHz (aliased at 16.6 kHz), which is outside the spectral range of this figure. 20.9 kHz is broadcast by the HWV transmitter in France, and its radiation pattern is clearly visible centered 900 km south and 400 km west of DHO (at the origin). However, a second enhanced region of energy appears about 300 km south of the origin, which corresponds to the area above the DHO transmitter (after accounting for propagation along the magnetic field line). It thus appears that the heating from the DHO transmitter is modifying the ionosphere, which subsequently affects the trans-ionospheric propagation of the HWV transmitter signal crossing through. The enhancement in the electric field is as high as 10–20 dB, and is shown with an arrow in the upper panel, though it is not detectable in the less sensitive magnetic field measurement. This observation is similar to the observation that VLF transmitter heating allows penetration of MF (1–3 MHz) signals from lightning through the ionosphere, as described by *Parrot et al.* [2009].

3. Discussion

[21] Figure 5 shows a scatterplot of the average amplitudes of the NWC signal for passes within the 150 km radius circle shown in Figure 2, as a function of the geomagnetic k_p index. Although the DEMETER mission corresponded largely to an extended solar minimum, there was still enough instances of elevated geomagnetic activity to observe trends in transmitter amplitudes in space with k_p indices as high as 6–8. The four panels show the electric field values (top row), magnetic field values (bottom row), nighttime measurements (left column) and daytime measurements (right column). None of the plots show a significant dependence or correlation with changing geomagnetic conditions. Though not shown, we also looked for correlations with the k_p index as far as two days prior to the satellite passes, and found no correlations for any amount of delay. As such, we conclude that the power injected into the magnetosphere from VLF transmitters is largely independent of geomagnetic conditions. Furthermore, the ionospheric absorption of VLF transmitter signals does not appear to strongly vary with geomagnetic activity, at least as measured by k_p. Recent analysis of DEMETER data have shown variations in ELF/VLF signals from lightning over the lifetime of the mission, which may be a result of the solar cycle activity impacting the ionosphere [*Toledo-Redondo et al.*, 2012]. We do not find a similar trend in VLF transmitter amplitudes, even though the lightning activity analyzed by *Toledo-Redondo et al.* [2012] is dominated by the same mid latitude region ($L < 2.6$) as the set of transmitters discussed here.

[22] Figure 6 shows the variation of the signal in the conjugate region with geomagnetic activity. As discussed

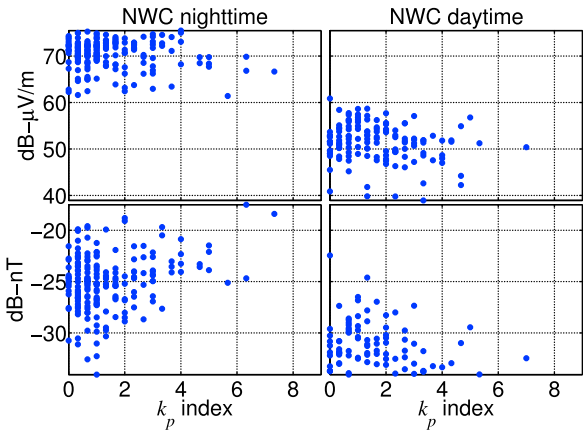

Figure 5. The variation with geomagnetic index k_p of the amplitude of NWC for all passes coming within the 150 km circle pictured in Figure 2 (bottom right). (top) Electric field, (bottom) magnetic field, (left) nighttime, and (right) daytime.

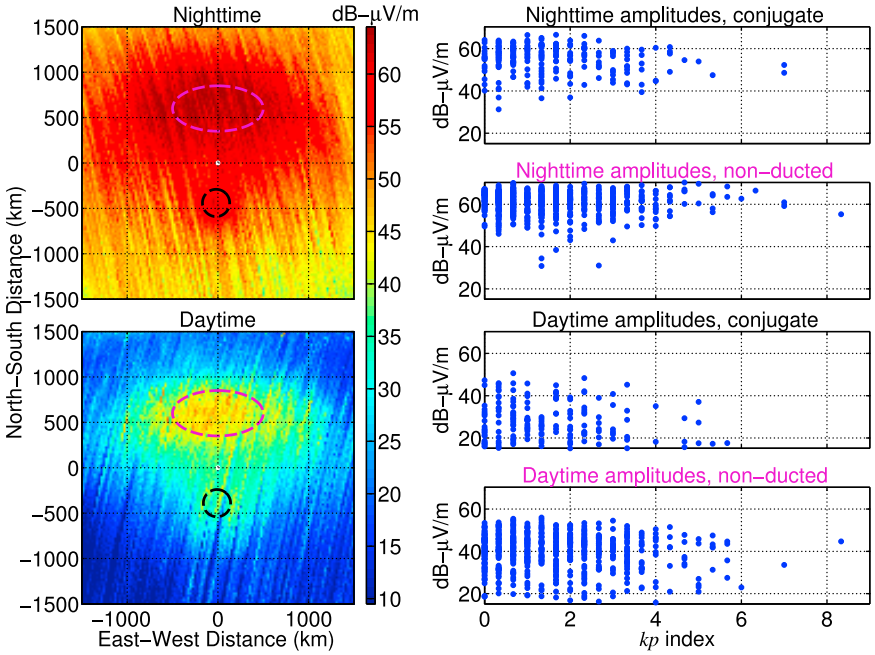

Figure 6. The electric field amplitudes of DEMETER passes in the conjugate hemisphere to NWC. (left) The radiation pattern at the conjugate hemisphere for (top) nighttime and (bottom) daytime. The dashed ellipses show a region encompassing the high-amplitude regions in the non-ducted zone (magenta) and the conjugate spot (black). The right four panels show a scatterplot of the amplitudes of all DEMETER passes through one of these regions, as a function of k_p index, separately plotted for daytime, nighttime, and the two conjugate regions.

earlier, we demarcate two distinct regions of radiation arriving in the conjugate hemisphere from NWC. The first, shown with a black circle, is centered near the conjugate point of the NWC signal shown in Figure 1, and has a radius 150 km. This region represents the radiation that has been scattered in the ionosphere to high wave normal angles, as well as any small amounts of ducted energy. The second larger region, shown with a magenta ellipse, is centered 1000 km poleward of the smaller spot, and represents the non-ducted propagation.

[23] For each satellite pass through one of these regions, the average amplitude during the pass within the region is calculated. The right panels of Figure 6 shows a scatterplot of the average electric field amplitudes as a function of k_p index, for both regions of propagation, and for both day and night measurements. We observe no obvious trend of the signal with increasing geomagnetic activity. We note that the power reaching the conjugate region is in part a function of the amount of wave growth resulting from gyroresonant interactions with energetic hot electrons (>1 keV) near the equator. For instance, VLF transmitters observed at the conjugate point on the ground have been shown to exhibit the effects of growth and triggered emissions [*Helliwell*, 1965, p. 279], particularly when ducts guide the transmitter signal along geomagnetic field lines. However, the steadiness of the signal in the conjugate region with geomagnetic activity observed here indicates that either the amount of wave-particle interactions leading to growth is independent of k_p index, or that the growth in general is too small to appreciably affect the average VLF transmitter power reaching the conjugate hemisphere.

[24] Although the observations in Figures 5 and 6 are only for NWC at $L = 1.4$, we repeated these observations for the other transmitters listed in Figure 1. Unfortunately, the NAA signal in the conjugate point is too weak due to the aliasing effect, but for the other transmitters, as high as $L = 2.6$, we found identical results: no correlation between k_p index and signal intensity. We cannot comment on how transmitter injection at high latitude may vary with geomagnetic conditions, but our results appear to be valid for low and mid latitudes.

[25] Since DEMETER survey mode records a horizontal component of both the electric and magnetic fields, it is possible to estimate the power flux and thus the total power radiated in the ionosphere from VLF transmitters. We assume that the unmeasured component of both the electric and magnetic fields are equal in magnitude to the measured component, due to circularly polarized propagation, in which case the Poynting flux ($\vec{S}_{av}$) can be estimated as

$$\vec{S}_{av} = 2|\vec{E}_{ICE} \times \vec{B}_{IMSC}| \quad (1)$$

where $\vec{E}_{ICE}$ and $\vec{B}_{IMSC}$ are the measurements of the electric and magnetic fields made by DEMETER, respectively, and the factor of $\frac{1}{2}$ in the usual Poynting flux equation is replaced by a factor of 2 because DEMETER only captured one quarter of the power (half the power in each of the electric and magnetic field, or one of the two horizontal components of each). Figure 7 shows the inferred Poynting flux above NWC for both daytime (top panel) and nighttime (bottom panel). It should be noted that because we have only single

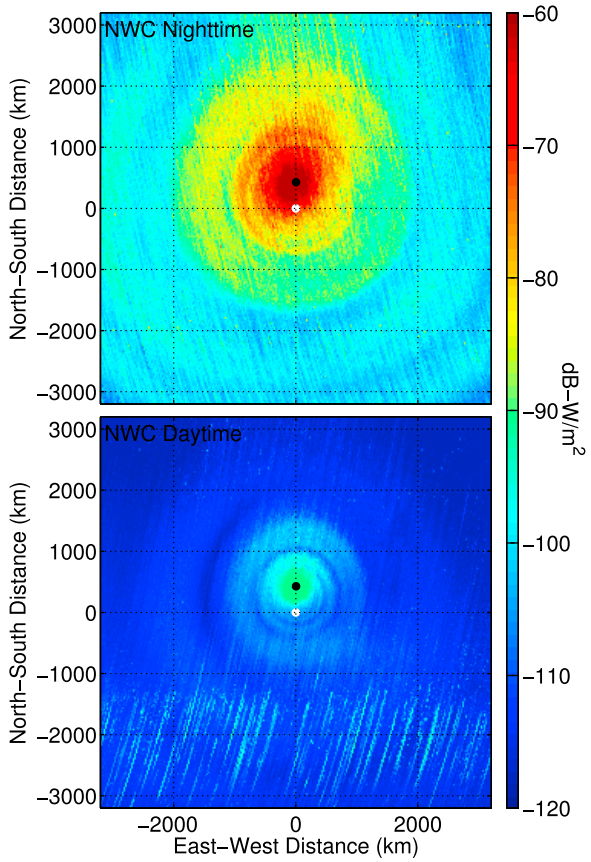

Figure 7. The Poynting flux calculated form one component of the electric and magnetic field, as in equation (1), for (top) nighttime NWC measurements and (bottom) daytime NWC measurements.

point measurements, and only one component of the electric and magnetic fields, we cannot distinguish the degree to which the observed fields (particularly the electric field) contain quasi-electrostatic energy propagating with high attenuation and a high wave normal angle at close to the resonance cone. However, as shown in Figure 3, the E/cB ratio is not systematically different between the two regions of propagation, leading to the suggestion that the bulk of the energy observed as the NWC signal emerged from the ionosphere is propagating (whereas the quasi-electrostatic waves would have a much higher E/cB ratio).

[26] Figure 8 shows the Poynting flux based on averaged DEMETER survey mode data, for all the transmitters listed in Table 1, for nighttime. We include all nine combinations of the three Russian alpha transmitters at the three different frequencies. The Russian alpha transmitters broadcast with a repeating 3.6 second format, divided into six 0.6-second segments. Each segment includes a 0.4-second pulse and a 0.2-second off time. The last two 0.6-second segments are quiet. There are three frequencies, ∼14.88, ∼12.65, and ∼11.91 kHz. Over the six segments, the Komsomolsk (KOM) transmitter broadcasts as follows: Off, 14.88, 12.65, 11.91, off, off. The Novosobirsk (NOV) transmitter broadcasts as follows: 11.91, 12.65, 14.88, 14.88, off, off. The Krasnodar (KRA) transmitter broadcasts as follows: 14.88, off, 11.91, 12.65, off, off. Because the 3.6 second pattern repeats reliably, only the DEMETER passes over a Russian alpha transmitter during a broadcast are taken, and the resulting power adjusted by the duty cycle so that the power plotted represents the average magnetospheric illumination when the transmitter is on.

[27] Direct calibration for transmitters above 20 kHz is not available, because the sampling frequency is 40 kHz, and the instrument voltage response was only available up to the Nyquist frequency. However, transmitters broadcasting above the Nyquist frequency are still detected in the data due to aliasing into the passband, for instance, NPM at 21.4 kHz can be detected at 18.6 kHz. The response of the instrument is extrapolated beyond 20 kHz with an exponential fit, to estimate the gain at the frequencies above 20 kHz. We then multiplied the observed power fluxes on DEMETER by the factor $(A(f_{tx})/A(40\ kHz - f_{tx}))^2$, where $A(f_{tx})$ is the extrapolated voltage response at the transmitter frequency. The values of $A(f_{tx})$ above the Nyquist frequency are estimated as follows: 1.17 at 20.27 kHz (ICV), 1.83 kHz at 20.9 kHz (HWU), 2.7 at 21.4 kHz (NPM), 3.75 at 22.2 kHz (JJI), and 10 at 24.0 kHz (NAA). However, because it relies on extrapolation of the amplitude response, the calibrated values for transmitters above 20 kHz, particularly NAA, are less accurate than the transmitters below 20 kHz. In addition, due to the multiplication by the scaling factor, the background noise level for the NAA transmitter is substantially higher.

[28] In each panel of Figure 8, the total power entering the magnetosphere is estimated by summing the Poynting flux within the dashed magenta circle. For nighttime measurements, the power within the circle is dominated by the transmitter signal, the effects of other VLF sources (like lightning) appear to be minimal. The total power injected by NWC into the magnetosphere is, on average, 125 kW, based on a circle 3000 km in radius, and centered at the point 440 km north of the location of NWC. This is at least a factor of two higher than any other transmitter injection observed here. The radiated power of NWC is 1 MW, meaning that ∼12.5% of the nighttime power escapes into the magnetosphere within a 3000 km radius, or a total power absorption of ∼9 dB. Although a full comparison to theoretical modeling is beyond the scope of this work, we do note that this value is very close to the ∼10 dB absorption estimated by *Helliwell* [1965, p. 71], for a geomagnetic latitude of 30°, and a VLF frequency of 20 kHz.

[29] The appropriate center points and radii of the magenta circles for the other transmitters are also determined visually, in order to capture as much of the transmitter power as possible without adding too much from either neighboring transmitters, or general background noise. For the ICV transmitter, the radius of the circle is 1000 km, to avoid including power from the GBZ transmitter, located to the northwest of ICV. ICV is also a weak transmitter (20 kW), injecting only 1848 W into the magnetosphere, or ∼9.2% of its nighttime power. The total power injected by the 7 MSK transmitters is ∼240 kW, although there are some very significant VLF transmitters that are not included here as their frequencies are too high above 20 kHz (like NLK at 24.8 kHz, and NLM at 25.2 kHz). The average total power of the Russian alpha transmitters observed in space, in their current transmission format is ∼8.6 kW.

[30] Figure 9 shows the same power flux and total power calculations for the daytime DEMETER passes. Due to higher

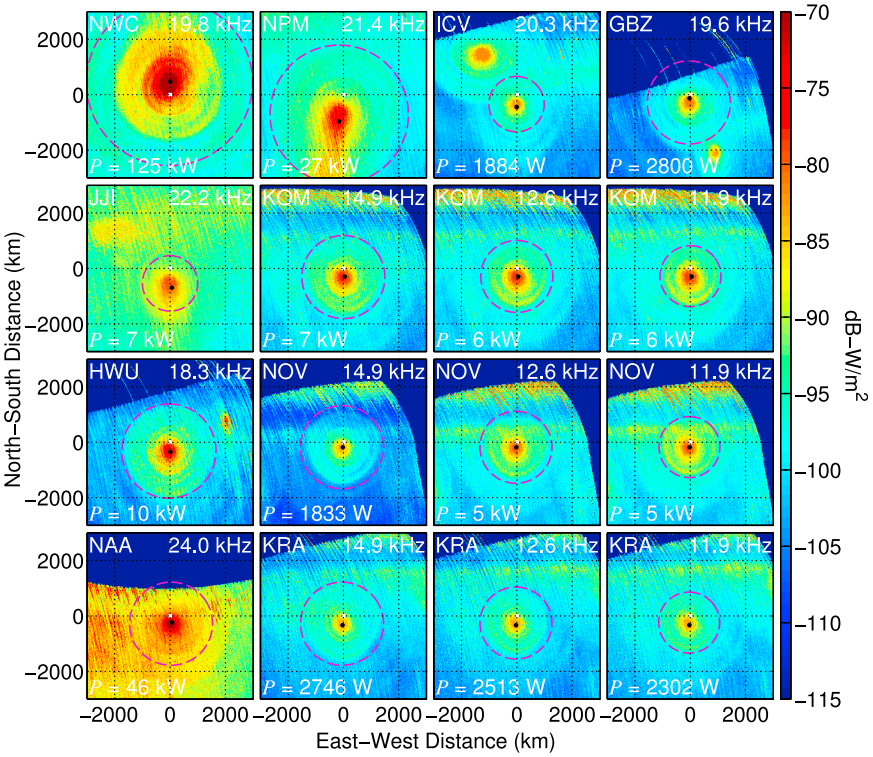

Figure 8. The Poynting flux from all VLF transmitters considered here, for the nighttime DEMETER passes. Magenta lines roughly bound the energy, and total power is calculated and displayed in the bottom left corner of each panel. The Russian 'Alpha' transmitters have been adjusted for duty cycle intrinsic in the transmission format, and the transmitters above 20 kHz have been adjusted by an estimated calibration factor to take into account their attenuation by the anti-aliasing filter.

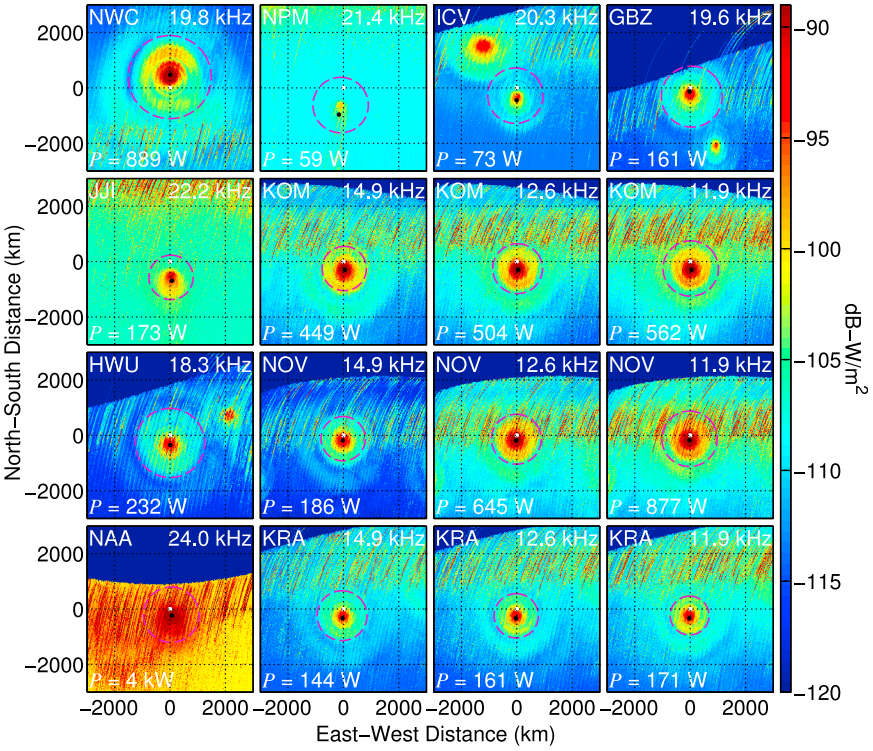

Figure 9. Same as Figure 8 but for daytime measurements.

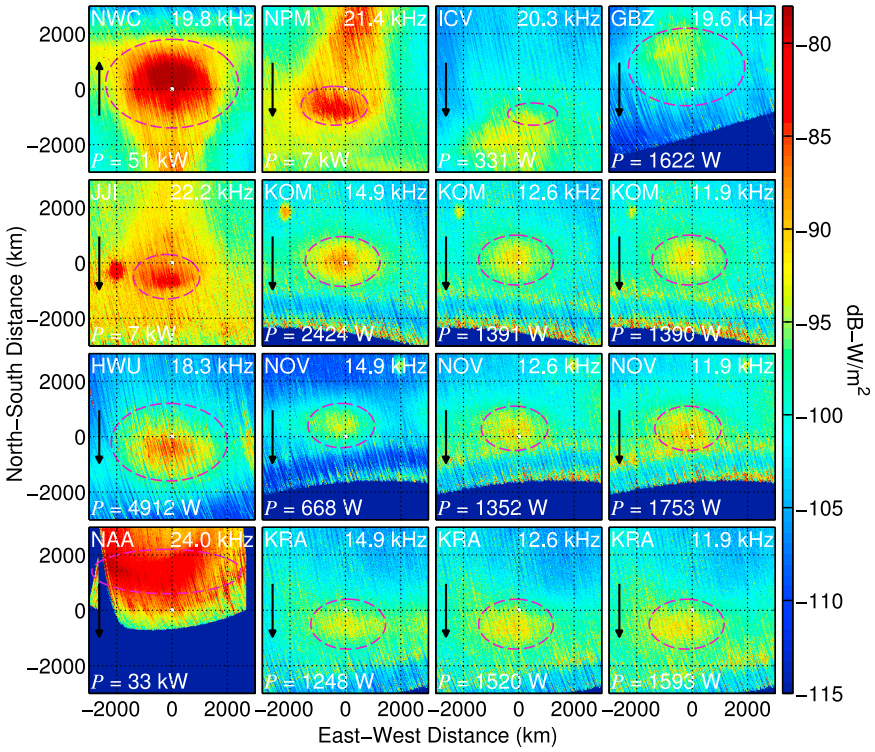

Figure 10. Same as Figure 8 but in the conjugate hemisphere. The arrows indicate the direction toward the geomagnetic pole.

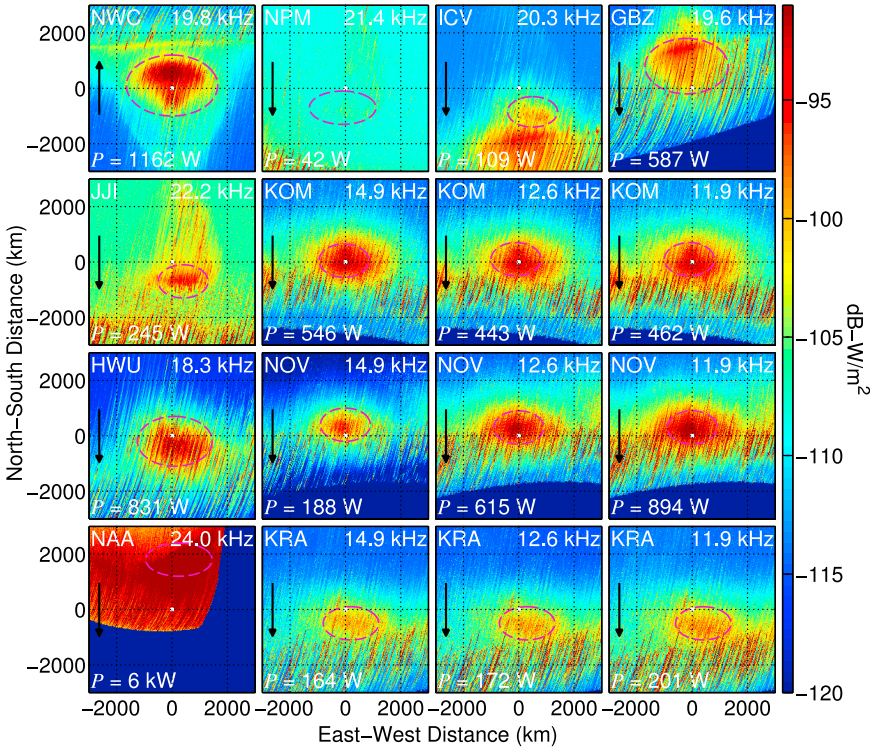

Figure 11. Same as Figure 9 but in the conjugate hemisphere. The arrows indicate the direction toward the geomagnetic pole.

electron densities in the *D*-region of the ionosphere from solar radiation, significantly less power reaches the magnetosphere. The radii of the circles used to calculate the total power is made smaller in the daytime due to weaker signals and stronger presence of lightning-generated sferic energy. The total power injected by NWC in daytime, for instance, is 990 W, within a 1500 km radius, or 21.5 dB lower than the nighttime value. The total power injected by the 7 MSK transmitters considered here is 1.6–7.6 kW. The NAA value of 6 kW is dominated by noise in the measurements due to the weak signal and attenuation in the anti-aliasing filter, which has raised the background levels substantially. If we assume the NAA nighttime signal was equally damped at daytime compared to daytime as were the other transmitters, the total injected energy from these transmitters is ∼2 kW, or ∼20 dB smaller than the nighttime power. However, the daytime total power of the Russian alpha transmitters is ∼930 W, only 10 dB smaller than the nighttime power.

[31] Figures 10 and 11 show the Poynting flux at the conjugate hemisphere of the same transmitters as in Figures 8 and 9, for nighttime and daytime measurements, respectively. For clarity, in each panel, an arrow indicates the direction toward the geomagnetic pole. Propagation from the VLF transmitter overhead region to the conjugate hemisphere includes Landau damping, which attenuates the wave as it approaches a high wave normal angle, as well as gyroresonant wave-particle interactions that can generate wave growth. One propagation phenomenon we rule out is that of magnetospheric reflection, which do not occur efficiently at these frequencies, all of which are well above the lower hybrid resonance in the ionosphere (5–9 kHz).

[32] For the nighttime VLF transmitters, a large fraction of the power is lost in reaching the conjugate hemisphere. For instance, the 125 kW of total power entering the magnetosphere above NWC reaches the conjugate region as only 50 kW of total power, representing more than a factor of two decrease, on average. The rest of the power may have been lost to Landau damping, either in the magnetosphere, or from scattered quasi-electrostatic waves emerging from the ionosphere. A complete theoretical explanation of the power radiation pattern at the conjugate hemisphere is beyond the scope of this paper, but further analysis with full wave modeling or raytracing may reveal the nature of the interhemispheric propagation of the transmitter signal.

[33] **Acknowledgments.** This work has been supported by AFRL award FA9453-11-C-0011 to Stanford University. We thank Denys Piddyachiy, Dave Lauben, Nikolai Lehtinen, Forrest Foust, Tim Bell, and Michael Starks for helpful discussions. We thank the DEMETER team, including Michel Parrot and Jean Jacques Berthelier, for helpful discussions and making the IMSC and ICE data available. k_p index data were taken from the NOAA National Geophysical Data Center ftp site. IGRF field information was taken from NASA GSFC Online calculator.

[34] Masaki Fujimoto thanks the reviewers for their assistance in evaluating this paper.

References

Abel, B., and R. M. Thorne (1998), Electron scattering loss in Earth's inner magnetosphere: 1. Dominant physical processes, *J. Geophys. Res.*, *103* (A2), 2385–2396.

Barr, R., M. T. Rietveld, H. Kopka, P. Stubbe, and E. Nielsen (1985), Extra-low-frequency radiation from the polar electrojet antenna, *Nature*, *317*(12), 155–157.

Bell, T. F., U. S. Inan, D. Piddyachiy, P. Kulkarni, and M. Parrot (2008), Effects of plasma density irregularities on the pitch angle scattering of radiation belt electrons by signals from ground based VLF transmitters, *Geophys. Res. Lett.*, *35*, L19103, doi:10.1029/2008GL034834.

Berthelier, J. J., et al. (2006), ICE, the electric field experiment on DEMETER, *Planet. Space Sci.*, *54*, 456–471.

Chrissan, D. A., and A. C. Fraser-Smith (1996), Seasonal variations of globally measured ELF/VLF radio noise, *Radio Sci.*, *31*(5), 1141–1152.

Clilverd, M. A., C. J. Rodger, R. Gamble, N. P. Meredith, M. Parrot, J. J. Berthelier, and N. R. Thomson (2008), Ground-based transmitter signals observed from space: Ducted or nonducted?, *J. Geophys. Res.*, *113*, A04211, doi:10.1029/2007JA012602.

Davies, K. (1990), *Ionospheric Radio*, *IEE Electromagn. Waves Ser.*, vol. 31, Peter Peregrinus, London.

Foust, F. R., U. S. Inan, T. F. Bell, and N. G. Lehtinen (2010), Quasi-electrostatic whistler mode wave excitation by linear scattering of EM whistler mode waves from magnetic field-aligned density irregularities, *J. Geophys. Res.*, *115*, A11310, doi:10.1029/2010JA015850.

Gemelos, E. S., U. S. Inan, M. Walt, M. Parrot, and J. A. Sauvaud (2009), Seasonal dependence of energetic electron precipitation: Evidence for a global role of lightning, *Geophys. Res. Lett.*, *36*, L21107, doi:10.1029/2009GL040396.

Gołkowski, M., U. S. Inan, A. R. Gibby, and M. B. Cohen (2008), Magnetospheric amplification and emission triggering by ELF/VLF waves injected by the 3.6 MW HAARP ionospheric heater, *J. Geophys. Res.*, *113*, A10201, doi:10.1029/2008JA013157.

Graf, K. L., U. S. Inan, and M. Spasojevic (2011), Transmitter-induced modulation of subionospheric VLF signals: Ionospheric heating rather than electron precipitation, *J. Geophys. Res.*, *116*, A12313, doi:10.1029/2011JA016996.

Helliwell, R., J. P. Katsufrakis, and M. L. Trimpi (1973), Whistler-induced amplitude perturbations in VLF propagation, *J. Geophys. Res.*, *78*(22), 4679–4688.

Helliwell, R. A. (1965), *Whistlers and Related Ionospheric Phenomena*, Dover, Mineola, N. Y.

Helliwell, R. A., and J. P. Katsufrakis (1974), VLF wave injection into the magnetosphere from Siple Station, Antarctica, *J. Geophys. Res.*, *79*(16), 2511–2518.

Inan, U. S. (1990), VLF heating of the lower ionosphere, *Geophys. Res. Lett.*, *17*(6), 729–732.

Inan, U. S., H. C. Chang, and R. A. Helliwell (1984), Electron precipitation zones around major ground-based VLF signal sources, *J. Geophys. Res.*, *89*(A5), 2891–2906.

Inan, U. S., M. Golkowski, M. K. Casey, R. C. Moore, W. Peter, P. Kulkarni, P. Kossey, E. Kennedy, S. Meth, and P. Smit (2007), Subionospheric VLF observations of transmitter-induced precipitation of inner radiation belt electrons, *Geophys. Res. Lett.*, *34*, L02106, doi:10.1029/2006GL028494.

Kulkarni, P., U. S. Inan, T. F. Bell, and J. Bortnik (2008), Precipitation signatures of ground-based VLF transmitters, *J. Geophys. Res.*, *113*, A07214, doi:10.1029/2007JA012569.

Li, X., et al. (2012), Study of the North West Cape electron belts observed by DEMETER satellite, *J. Geophys. Res.*, *117*, A04201, doi:10.1029/2011JA017121.

Parrot, M., et al. (2006), The magnetic field experiment IMSC and its data processing onboard DEMETER: Scientific objectives, description and first results, *Planet. Space Sci.*, *54*(5), 441–455.

Parrot, M., U. S. Inan, and N. G. Lehtinen (2008), V-shaped VLF streaks recorded on DEMETER above powerful thunderstorms, *J. Geophys. Res.*, *113*, A10310, doi:10.1029/2008JA013336.

Parrot, M., U. S. Inan, N. G. Lehtinen, and J. L. Pincon (2009), Penetration of lightning MF signals to the upper ionosphere over VLF ground-based transmitters, *J. Geophys. Res.*, *114*, A12318, doi:10.1029/2009JA014598.

Peter, W. B., and U. S. Inan (2007), A quantitative comparison of lightning-induced electron precipitation and VLF signal perturbations, *J. Geophys. Res.*, *112*, A12212, doi:10.1029/2006JA012165.

Piddyachiy, D., U. S. Inan, and T. F. Bell (2008), DEMETER observations of an intense upgoing column of ELF/VLF radiation excited by the HAARP HF, *J. Geophys. Res.*, *113*, A10308, doi:10.1029/2008JA013208.

Rodriguez, J. V., and U. S. Inan (1994), Electron density changes in the nighttime D region due to heating by very-low-frequency transmitters, *Geophys. Res. Lett.*, *21*(2), 93–96.

Shao, X., B. Eliasson, A. S. Sharma, G. Milikh, and K. Papadopoulos (2012), Attenuation of whistler waves through conversion to lower hybrid waves in the low-altitude ionosphere, *J. Geophys. Res.*, *117*, A04311, doi:10.1029/2011JA017339.

Starks, M. J., R. A. Quinn, G. P. Ginet, J. M. Albert, G. S. Sales, B. W. Reinisch, and P. Song (2008), Illumination of the plasmasphere by terrestrial very low frequency transmitters: Model validation, *J. Geophys. Res.*, *113*, A09320, doi:10.1029/2008JA013112.

Storey, L. R. O. (1953), An investigation of whistling atmospherics, *Philos. Trans. R. Soc. London A*, *246*, 113–141.
Swanson, E. R. (1983), Omega, *Proc. IEEE*, *71*(10), 1140–1155.
Tao, X., J. Bortnik, and M. Friedrich (2010), Variance of transionospheric VLF wave power absorption, *J. Geophys. Res.*, *115*, A07303, doi:10.1029/2009JA015115.
Toledo-Redondo, S., M. Parrot, and A. Salinas (2012), Variation of the first cut-off frequency of the earth-ionosphere waveguide observed by DEMETER, *J. Geophys. Res.*, *117*, A04321, doi:10.1029/2011JA017400.
Uman, M. A. (1987), *The Lightning Discharge*, Dover, Orlando, Fla.
Vampola, A. L. (1977), VLF transmission induced slot electron precipitation, *Geophys. Res. Lett.*, *4*(12), 569–572.
Watt, A. D. (1967), *VLF Radio Engineering*, Pergamon, Oxford, U. K.